Title: **Pan-retinal characterization of Light Responses from Ganglion Cells in the Developing Mouse Retina**

Abbreviated Title: **Pan-retinal Development of Light Responses**

Gerrit Hilgen[1*], Sahar Pirmoradian[2*], Daniela Pamplona[3], Pierre Kornprobst[3], Bruno Cessac[3,] Matthias H. Hennig[2], Evelyne Sernagor[1]

[1] Institute of Neuroscience, Newcastle University, Newcastle upon Tyne NE2 4HH, UK

[2] Institute for Adaptive and Neural Computation, University of Edinburgh EH8 9AB, Edinburgh, UK

[3] Inria, Neuromathcomp Team, 06902 Sophia Antipolis, France

* equal contributions

Corresponding author: Dr Gerrit Hilgen, Institute of Neuroscience, Newcastle University, Framlington Place, Newcastle upon Tyne NE2 4HH, UK, email: Gerrit.Hilgen@ncl.ac.uk

Number of pages: 32

Number of Figures: 7

Number of Tables: 1

Abstract Word Count: 246

Introduction Word Count: 506

Discussion Word Count: 1438

Conflict of Interest

The authors declare no competing financial interests.

Acknowledgements

This work was supported by RENVISION (EU Grant FP7-FET-NBIS). We thank Alessandro Maccione, Stefano di Marco and Luca Berdondini for designing and providing the visual stimulation system.

Abstract

The functional organization of the mammalian retina is not spatially uniform. These functional inhomogenities presumably represent adaptations to specific visual needs associated with particular ecological benefits. However, how such asymmetries develop has not been documented yet. Here we present the ontogeny of light responses in mouse RGCs from eye opening to adulthood. Using a large-scale, high-density multielectrode array, we were able to record simultaneously from hundreds to thousands of dorsal and ventral RGCs, documenting light response properties (firing peak amplitude, time to peak and response duration) for the three major RGC types (ON, OFF, ON-OFF). Responses to different contrasts not only revealed a complex developmental profile for all three RGC types, but also unveiled differences between RGCs located in the dorsal versus ventral retina. At eye-opening, dorsal RGCs of all types were significantly more responsive to light, perhaps indicating an ecological advantage to nest viewing for young, pre-weaning pups. At the same time, the developmental profile of ON and OFF RGCs exhibited antagonistic behavior, with the strongest ON responses shortly after eye-opening, followed by an increase in the strength of OFF responses at later stages. We estimated RGC receptive field sizes and polarity across development using a novel super-resolution approach based on white noise and spike-triggered average (STA) responses and found that receptive field centers decrease but STA strength increases with maturation. These results show for the first time that the refinement of developing RGC responses to light is also not spatially uniform across the retina.

Significance Statement (120 maximum)

Using a large-scale, high-density multielectrode array, we have investigated the ontogeny of light responses in retinal ganglion cells (RGCs) in the developing mouse retina. We were able to record from hundreds to thousands of RGCs simultaneously at pan-retinal level, and found that the refinement of receptive field properties strikingly differs between RGCs in the dorsal and ventral retina, with stronger ON and generally more prominent responses in the dorsal retina immediately after eye opening, followed by an increase in OFF responses. These findings suggest that retinal functionality is not spatially uniform and that there might be an ecological advantage to favoring the development of dorsal light responses before the rest of the retina reaches functional maturity.

Introduction

The onset of visual experience in the mouse occurs around postnatal day (P) 12, at eye opening. Although the retina cannot experience patterned vision before eye-opening, it is remarkable that as soon as visual experience begins, RGCs are already capable of encoding information originating from photoreceptors and transmit it to retinal central targets. However, these early light responses are far from mature looking, and they progressively acquire their adult features while the retina develops (Masland, 1977 (rabbit); Tootle, 1993 (cat); Sernagor and Grzywacz, 1995 (turtle); for review see Sernagor and Chalupa, 2006). In mouse, it has been demonstrated that RGC dendritic stratification in the ON and OFF layers of the inner plexiform layer matures after eye opening (for review see Tian, 2011) and light-driven activity guides the refinement of synaptic connectivity (Tian and Copenhagen, 2001, 2003). Consequently, receptive field (RF) sizes (Cantrell et al., 2010; Koehler et al., 2011) and complex RF properties such as direction and orientation selectivity (Elstrott et al., 2008; Chen et al., 2014) keep maturing after the onset of visual experience. Yet, despite ongoing maturation after eye opening, longitudinal studies of RF properties have been poorly documented (but see Sernagor and Grzywacz, 1995).

One important yet often neglected issue is that the retina is not uniformly organized from a functional perspective. Indeed, dorsal, ventral, nasal and temporal domains have evolved to enable optimal encoding of specific features in the visual scene. For example, mouse cones co-express medium wavelength opsin (M-opsin) and short wavelength opsin (S-opsin), with a dorsal-to-ventral increasing gradient in S-opsin (and opposite for M-opsin) (Szel et al., 1992; Röhlich et al., 1994; Szél et al., 1996; Applebury et al., 2000; Lukáts et al., 2005). These dorso-ventral gradients affect RGC responses in adult animals with respect to their spectral tuning (Ekesten and Gouras, 2005; Wang et al., 2011; Chang et al., 2013), improving encoding of achromatic contrasts (Yin et al., 2009; Baden et al., 2013) and providing evolutionary advantages for visual tasks (Peichl, 2005). Another feature of retinal dorso-ventral non-uniformity is the topographical density of some RGC subtypes (Zhang et al., 2012; Bleckert et al., 2014). However, nothing is known about the developmental aspects of these inhomogeneities.

Here we present a longitudinal study of RGC RF properties in the developing mouse retina from eye opening up to maturity with emphasis on dorso-ventral topographical differences. We recorded

simultaneously from hundreds to thousands of RGCs at near pan-retinal level using the high-density large-scale CMOS-based Active Pixel Sensor multielectrode array (APS MEA) (Biocam, 3Brain) featuring 4096 electrodes (42 µm pitch) arranged in a 64x64 configuration, covering an active area of 7.12 mm^2 (Berdondini et al., 2009; Maccione et al., 2014), allowing us to discriminate topographical differences in light responses in individual retinas. We classified RGCs as ON, OFF and ON-OFF, measuring their basic firing properties such as latency, peak amplitude and response duration at different contrast levels. We completed our study by determining the spatio-temporal properties of the RF central areas in these cells throughout development using a new, high resolution reverse correlation approach.

Materials & Methods

Retina Preparation

Experimental procedures were approved by the UK Home Office, Animals (Scientific procedures) Act 1986. Wild-type mice (C57bl/6) of either sex, housed under a 12 hour light-dark cycle and aged between postnatal days (P) 13-63 were used for the experiments. Mice were dark-adapted overnight and killed by cervical dislocation. Eyes were enucleated, and following removal of the cornea, lens, and vitreous body, they were placed in artificial cerebrospinal fluid (aCSF) containing the following (in mM): 118 NaCl, 25 $NaHCO_3$, 1 NaH_2PO_4, 3 KCl, 1 $MgCl_2$, 2 $CaCl_2$, 10 glucose, and 0.5 l-Glutamine, equilibrated with 95% O_2 and 5% CO_2. The ventral and dorsal orientation was marked after enucleation and confirmed by using vascular landmarks in the retina (Wei et al., 2010) The retina was isolated from the eye cup and flattened for MEA recordings and the ventral-dorsal, nasal-temporal orientation was noted down. All procedures were performed in dim red light and the room was maintained in darkness throughout the experiment.

MEA recordings

The isolated retina was placed, RGC layer facing down, onto the MEA and flattened by placing a small piece of translucent polyester membrane filter (Sterlitech Corp., Kent, WA, USA) on the retina followed by a home-made anchor. Pan-retinal recordings were performed on the BioCam4096 platform with BioChips 4096S+ (3Brain GmbH, Lanquart, Switzerland), integrating 4096 square microelectrodes (21

× 21 μm, pitch 42 μm) on an active area of 2.67 × 2.67 mm. The platform records at a sampling rate of 7.1 kHz/electrode when using the full 64×64 array and recordings were stored at 12 bits resolution per channel with a 8 kHz low-pass filter/0.8 Khz high-pass filter using 3Brain's BrainWave software application. Throughout recording, retinas were maintained at 33°C using an in-line heater (Warner Instruments LLC, Hamden, CT, USA) and continuously perfused using a peristaltic pump (~1 ml min^{-1}). To reliably extract spikes from the raw traces we used a quantile-based event detection (Maccione et al., 2014; Muthmann et al., 2015) and single-unit spikes were sorted using the T-Distribution Expectation-Maximization algorithm in Offline Sorter (Plexon Inc, Dallas, USA). Sorted units that exhibited at least >0.1 spikes/sec on average over the entire recording session were then verified by visual inspection of the detected clusters in the 2/3D principal component feature space, the calculated cluster inter spike intervals with respect to the refractory period and the shape of the spike waveforms in the Offline Sorter GUI. Due to the high density of the electrodes, the same units were sometimes detected on multiple neighboring channels. These redundant units were removed by comparing coincident spikes between neighboring units. Briefly, for each unit, spikes occurring within +-2 frames (1 Frame = 1/7.06 ms) were detected in all units on the four closest electrodes and marked. This was done for all units, and units with more than 5% coincident spikes were iteratively removed such that for each coincident group only the one with the largest spike count was retained.

Light Stimulation

The light stimulation system is based on a DLP video projector ("lightCrafter", Texas Instruments, USA), and was designed to project visual stimuli above the photoreceptor layer with micrometer spatial resolution over the entire retina. The total area covered by the light patterns is 664×664 pixels and each light-pixel covers 4×4μm^2 of the chip active area. The sync signal from each frame is integrated with the BioCam system and synchronizes the light stimuli with the electrophysiological responses recorded from the RGCs. Light stimuli were attenuated using neutral density filters to high mesopic light levels (mean luminance 11 cd/m^2).

Full Field stimuli

A full field stimulus that switched from light to dark (0.5 Hz, 30 repetitions) was used to define peak response latency, duration and relative amplitude of ON and OFF responses (see Fig. 1A). The

luminance contrast for this stimulus measured as the Michelson contrast was defined as ($I_{max} - I_{min}$)/($I_{max} + I_{min}$) where I_{max} and I_{min} are respectively the maximum and minimum luminance and had a maximal value of 0.70. We also used full field stimuli with a series of increasing Michelson contrasts (0.19, 0.41, 0.53, 0.62, 0.67). We estimated each unit's instantaneous firing rate for the different full field intensities by convolving its spike train with a Gaussian kernel smoothing function (standard deviation = 25ms). We then averaged the trials (Fig. 1A) and extracted several features like the amplitude of ON and OFF responses (*A1, A2*), the time to these response peaks from stimulus onset or offset (*T2P1, T2P2*) and the response duration (*RD1, RD2*). Statistical significance was evaluated using One-way ANOVA with a Bonferroni post-hoc test (Prism, GraphPad, CA).

To classify RGCs according to their main response polarity, we measured the relative amplitude of ON and OFF responses and calculated the *Bias Index* (*BI*) defined as (*A1 – A2*)/(*A1 + A2*) (Carcieri et al., 2003). We used the *BI* to classify the cells into OFF (*BI* -1 to -0.33), ON-OFF (*BI* -0.33 to 0.33) and ON cells (*BI* 0.33 to 1).

To estimate the variability of the spike count between trials at different developmental stages, we calculated the Fano Factor (*F*), defined as the variance (σ^2) of the spike count during a given time bin (*W*) divided by the mean (μ) spike count over that same time bin.

$$F = \frac{\sigma_W^2}{\mu_W} \quad (1)$$

We binned the full field response length (4 sec) into 25 ms time windows and calculated *F* for all time windows. We then averaged the *F* values for all cells from the same age and RGC type.

Shifted White Noise

Checkerboard stimuli are routinely used to measure RF areas (Rieke et al., 1997; Chichilnisky, 2001). Finer resolution can be achieved using smaller unitary checkerboard pixels, but at the same time very small checkerboard pixels may not be able to elicit reliable and repeatable responses, if at all, necessitating to reach a trade-off. Here we use an improved checkerboard stimulus, so-called shifted white noise (SWN), where checkerboard pixels are shifted randomly in space at fixed time steps (Pamplona et al., 2015). With this novel approach, the checkerboard pixel size is large enough to

reliably evoke significant responses, but at the same time, the RF resolution can be very fine, given by the shift size (Fig. 1B). The SWN images I_ε are defined as:

$$I_\varepsilon(x,y,t) = \sum_{b=1}^{B} \Pi_P\big(x - X_b - \varepsilon_S(x,t)\big)\Pi_P\big(y - Y_b - \varepsilon_S(y,t)\big)\omega(b,t) \quad (2)$$

Images are composed of B checkerboard pixels with a fixed size P, the area of each pixel is denoted by a rectangular function Π_P, b is the block index and its top left corner coordinates are (X_b, Y_b). The index of each pixel is given by the random variable $\omega(b,t)$ which is taken from a Bernoulli distribution of values -1 (color black) and 1 (color white) with equal probability 0.5 for each block b at each time stamp t. Each image is randomly shifted horizontally (shift $\varepsilon_x(t)$) and vertically (shift $\varepsilon_y(t)$). The shifts $\varepsilon_x(t)$ and $\varepsilon_y(t)$ are random variables taking S possible values with a probability $1/S$. Here we take S=4. They are redrawn at each time step. We used 17 x 17 pixels (B = 289) with an edge size of 160 µm (P = 160) and a shift step size of P/4 (40 µm) and we considered 4 steps (S = 0, 40, 80, 120) both for horizontal and vertical shifts. The Michelson contrast was 0.7 with the same mean luminance stated before and SWN images were presented for 33 ms each (30 Hz, ~45 min, ~15 min for adult retinas). The spike triggered average (STA) (Chichilnisky, 2001) was calculated by computing the average stimulus 500 ms (corresponding to 15 checkerboard frames) before a spike occurred. At the time point of the positive or negative peak maximum of the average temporal STA, a two-dimensional Gaussian was fitted to the corresponding spatial profile frame and an ellipse was circled around the center with 1 SD of the Gaussian fit. The RF diameter was defined as the diameter of a circle with the same area as the ellipse (2*radius = 2 SD).

Results

The spatial extent (2.67 x 2.67 mm) of the active area of the APS MEA chip allowed us to record simultaneously from dorsal and ventral RGCs over large retinal areas (Fig. 2A). The small electrode pitch (42 µm) of the APS chip enables sampling from many individual RGCs from these areas, providing us with an unbiased large sample size for all analysis presented here (see Table 1). Figure 2A

shows that it is possible to visualize the outline of the retina, to quantify activity levels on individual channels and to delineate various retinal areas on the MEA chip simply by looking at spiking activity (spike count). For each channel the log spike count of a full field stimulus experiment (see Methods) from a P13 and a P38 retina were pseudo color-coded and plotted according to their position on the 64x64 MEA (Fig. 2A). This generates activity maps showing that the outline of the P13 retina is smaller compared to the P38 retina and that the spike rate is overall higher in all channels in that younger retina. Figure 2B illustrates responses to these same full-field stimuli in both retinas following spike sorting and classification (see Methods), yielding spike rasters and histograms for dorsally and ventrally located ON (green), OFF (red) and ON-OFF (blue) RGCs (Fig. 2B). The responses of P13 ON cells to the alternating full field stimulus were much stronger and were more sustained compared to the responses of OFF and ON-OFF RGC types in the same retina (Fig. 2B top) and to all responses in the P38 retina (Fig. 2B bottom). OFF and ON-OFF cell responses more defined at P38 compared to OFF and ON-OFF responses at P13. Interestingly, the ON cell responses were stronger in the dorsal part of the retina than in the ventral part (Fig. 2B top, compare left and right). In contrast, at P38, ON responses were somewhat stronger and brief in the ventral part (Fig. 2B bottom right) compared to the dorsal part, whereas it was the opposite for OFF responses (Fig. 2B bottom left).

This simple visualization demonstrates that the development of basic firing properties varies not only for different RGC types but even for ON and OFF RGCs located in dorsal versus ventral locations. Next, we quantified these stimulus-driven responses for different RGC types and different ages (Fig. 3), and we examined how these responses change when the full-field stimulus was presented with different Michelson contrasts (Fig. 4-6).

Ontogeny of dorsal and ventral light response features for different RGC types

Full field stimuli were presented to retinas of different ages and post-stimulus time histograms (PSTH) were generated for every RGC. The results were classified into 4 age groups: P13 (4 retinas, 4183 RGCs in total), P16/P17 (2 P16 and 2 P17 retinas, 4404 RGCs), P19 (3 retinas, 3210 RGCs) and P29/P38 (2 P29 and 2 P38 retinas, 5811 RGCs) and further divided into dorsal (green) and ventral (blue) located units. For the rest of the manuscript we are referring to these same groups (Table 1). From individual

PSTHs, we extracted the peak amplitude, time to peak and response duration for light onset and offset (see Fig. 1A) and RGCs from each age group were classified into ON, OFF and ON-OFF cells according to the *Bias Index* (see Methods). Fig. 3A summarizes results for all RGCs at all ages, illustrating the dorsal (green) and ventral (blue) mean peak amplitude A1 in ON cells (left), A2 in OFF cells (middle) and A1+A2 in ON-OFF cells (right), where A1=solid and A2=dotted line.

In line with the observations from the individual retinas in Fig. 2B, dorsal P13 ON cells (Fig. 3A, left) were significantly more active than OFF and ON-OFF cells at eye-opening, in both dorsal and ventral areas Dorsal ON cells also showed a progressive decrease in their mean peak amplitude whereas OFF (dorsal and ventral) cells showed an increase from P13 to P29/P38 (Fig. 3A, middle). Dorsal OFF cells showed, except for P13, significant higher peak rates than ventral OFF cells. ON-OFF cells, on the other hand, did not show significant changes between the youngest and oldest age groups and their responses were overall weaker compared to the other cell types (Fig. 3A, right).

How brisk these responses to full field stimuli are at different ages was evaluated by measuring the time from stimulus on- or offset to the peak amplitude (*T2P1* and *T2P2*, respectively). We found that the mean time to peak is progressively decreasing from P13 to P29/P38 both for ON and OFF cells, with the OFF cells exhibiting slower response onsets than the ON cells (Fig. 3B, middle). ON-OFF cells had slower response onsets than ON and OFF cells. Overall it seemed that ventrally located RGCs had slightly slower times to peak than ventral RGCs.

How sustained or transient a RGC response is, was defined by measuring the response duration following the peak (see Fig. 1A, *RD1, RD2*). The spike rasters in Fig. 2B clearly show that dorsal ON cells respond in a much more sustained fashion at P13. This observation was confirmed by plotting the dorsal and ventral mean response duration values at this age (Fig. 3C, left), revealing that dorsal ON responses were significantly more sustained at P13. After P13, dorsal and ventral ON responses showed no differences anymore and the response duration gradually drops down until adulthood (Fig. 3C, left). In contrast, OFF cells become moderately more sustained between P13 and 38 and eventually, they end up becoming slightly longer than ON responses in adulthood (Fig. 3C, middle). Interestingly, response durations reach a peak at P16-P19. Finally, the overall durations of ON-OFF responses were lower

compared to the other types, with no major changes associated with maturation (Fig. 3C, right) and the only difference between dorsal and ventral cells was found at P13.

The PSTH gives a measure of averaged responses over all trials for individual RGCs. To evaluate the variability of the individual RGC responses, we calculated the Fano factor (see Methods) for all cells from P13 to maturity. Higher Fano factor values correspond to responses with greater variability. Figure 3D illustrates that the Fano factor values are consistently higher at P13 for all three cell types and they become smaller with retinal maturation. Fano factor values are overall lower for ON cells, especially for the time after stimulus on- and offset.

Taken together, the peak amplitudes and response durations of ON and OFF cells showed an antagonistic behavior from eye opening to maturity (with developmental changes in ON cells most dramatic) whereas the ON-OFF cell responses exhibit less developmental variability. Response variability decreases across trials as the retina matures.

Ventral and dorsal difference – Peak Amplitude

Next, we investigated whether the developmental changes described above differ for different contrasts in the ventral and dorsal areas of the retina. We used the same age groups as above and looked at full field responses with different Michelson contrasts (see Methods). Figure 4A illustrates the firing peak amplitude values for all ON cells (*A1*) from a P13 retina for three different full field contrasts (0.41, 0.53, 0.62) plotted with respect to their electrode position on the array. Overall, the dorsal side clearly shows stronger activity than the ventral side, especially for MC 0.62. To establish whether this dorsal-ventral trend is present in all retinas of the same age group and/or between the age groups, we calculated the mean peak amplitude values for all full field contrasts for ON (Fig. 4B top), OFF (Fig. 4B middle) and ON-OFF (Fig. 4B bottom) RGCs and all age groups (Fig. 4B) with respect to their dorsal (green) or ventral (blue) position. At P13, ON dorsal RGCs exhibited significantly higher peak firing rates than ON ventral cells at all contrast levels (Fig. 4B top left). Similarly, P13 OFF and ON-OFF cells located in the dorsal part of the retina also had significantly higher peak firing rates at most contrast levels (Fig. 4B middle and bottom left) than their ventral counterparts. Interestingly, the highest values and most pronounced differences between dorsal and ventral cells were observed at 0.62 Michelson contrast

277 rather than at high contrast (0.7). At P16/17 and P19, dorsal OFF RGCs were also significantly more
278 active than their ventral counterparts (Fig. 4B middle), whereas there were no significant differences
279 between dorsal and ventral ON and ON-OFF cells (Fig. 4B top and bottom). At P19, ventral ON cell
280 peak amplitudes became significant higher than the dorsal ones for the three strongest contrast levels
281 whereas that trend moved towards lower contrast levels in adult retinas and virtually disappeared at
282 high contrasts (Fig. 4B top right). A similar antagonistic behavior of the dorsal-ventral response strength
283 for increasing contrasts was observed for adult OFF RGCs (Fig. 4B middle right). Interestingly, and in
284 contrast to P13 ON-OFF amplitudes (Fig. 4B bottom left), ventral adult ON-OFF cells were
285 significantly more active (for both *A1* and *A2*) than their dorsal counterparts at all but the weakest
286 contrast levels.
287
288 **Ventral and dorsal difference – Time to Peak**
289 Time to peak responses also exhibited significant differences between dorsal and ventral areas and
290 between different age groups. Figure 5A shows time to peak values (*T2P2*) for all OFF cells from a
291 mature P38 retina for three different full field contrasts (0.19, 0.53, 0.7). Here, responses seem to take
292 longer to develop (larger time to peak values) for lower contrasts. Similar trends were observed for
293 adult ON cells (Fig. 5B top right), with dorsal RGCs showing significantly longer times to peak than
294 ventral cells for up to 0.62 Michelson contrast levels. On the other hand, there were no differences
295 between dorsal and ventral ON cells at P19 and P16/P17 (Fig. 5B top middle). As a matter of fact, the
296 only additional significant differences observed for ON cells were at P13, with longer times to peak for
297 ventral cells at the three highest Michelson contrast levels (Fig. 5B top left). In line with ON cells,
298 dorsal adult OFF RGCs had longer time to peak values than ventral cells for up to 0.62 Michelson
299 contrast levels (Fig. 5B middle right). At P13 there were no differences between the dorsal and ventral
300 sides (except for 0.67 Michelson contrast level) (Fig. 5B middle left). For both P16/17 and P19,
301 responses were longer to develop for ventral RGCs at most contrast levels. As for ON-OFF cells,
302 dorsally located cells had longer time to peak values than ventral cells in adult retinas but not in younger
303 retinas, with the exception of larger values for the OFF component (*T2P2)* in ventral cells at P13 (Fig.
304 5B bottom left).

Ventral and dorsal difference – Response Duration

There were also differences with respect to cell location and age for the duration of responses to full field flashes. Figure 6A illustrates response durations for all ON cells in a P13 retina for three different contrast levels (0.19, 0.62, 0.7), with longer responses developing at higher contrasts in the dorsal part of the retina. These observations are summarized for all P13 retinas in Fig. 6B (top left). P13 OFF cells (Fig. 6B middle left) and ON-OFF cells (Fig. 6B bottom left) showed a similar trend, with longer response durations in dorsal cells for most contrast levels. There was a similar trend for ON cells at P16/17 (Fig. 6B, top middle). In contrast, the trend was inverted for OFF cells at P16/17, with longer responses in dorsal cells than in ventral cells. As for adult retinas, differences between dorsal and ventral cells become virtually non-existent, except for small differences at higher contrast levels (e.g. longer ventral OFF responses at 0.7 contrast level at P19; longer dorsal OFF responses at contrast levels 0.62, 0.67 and 0.7 in adult retinas).

In summary, there are significant differences between the dorsal and ventral response properties for different RGC types from eye-opening to maturity. Shortly after eye opening (P13), dorsal RGCs exhibit much stronger and more sustained responses to full field flashes than ventral cells. This dorsal-to-ventral difference fades as development progresses, and for ON-OFF cells the gradient even reverses to ventral-to-dorsal. The dorsal-to-ventral difference is present at later developmental stages for temporal response features such as time to peak, with dorsal RGCs exhibiting much slower responses than ventral cells at low contrast levels.

Maturation of RGC RF centers

We used a novel checkerboard stimulus, the shifted white noise (SWN, see methods), to characterize the maturation of ON and OFF RGC RF centers from eye-opening to maturity using STA analysis. The STA is the mean stimulus that precedes a spike, and SWN enables mapping RFs with higher resolution than ordinary checkerboard patterns. Panels A and C in Figure 7 respectively show the STA time courses and their spatial profiles with the fitted corresponding RF for selected example cells (ON in Panel A and OFF in Panel C) for all age groups. On the temporal STA, we quantify the signal strength

by measuring the STA amplitude (the deviation in either directions from the mean (0.5 pixel intensity as a fraction)). The cell type is inferred from the STA polarity for the phase closest to the spike time 0 (negative for OFF (blue) and positive for ON (yellow) RGCs). The most striking developmental change that can be observed in these figures is that STA values are much smaller at P13-16 than later during development. For example, both phases of the STA for an ON (Fig 7A) and an OFF (Fig 7C) RF center are small at P13 and P16 compared to P19 and adult (P44 and P63). The ON and OFF STA amplitudes from these examples are slightly higher in adults compared to P19. In addition, the duration of the STA decreases with development, consistent with our findings for responses to full field flashes.

We next used the STA responses to measure RF diameters and quantify their developmental changes from eye-opening to maturity. Figure 7B illustrates developmental changes in RF diameters as box plots of all ON cells (yellow boxes; P13-N=2 retinas, n = 449 cells; P16-N=2, n=425; P19-N=2, n=926; adult-N=2; n=698) and separately for dorsal and ventral RGCs (black boxes). RF diameters are largest at P13, and then drop down to a minimum at P16, followed by a marginal, non-significant increase at P19 and then a more significant increase from P19 to adulthood. Since we observed significant differences in firing properties between dorsal and ventral RGCs, we also looked at RF sizes separately for these same two groups, but we found no major differences between ventral and dorsal cells (except for adult, where ventral RFs diameters were significantly larger than dorsal ones). Figure 7D illustrates the same for all OFF cells (blue boxes; P13-N=2, n=309; P16-N=2, n=239; P19-N=2, n=794; adult-N=2, n=514)) and separately for dorsal and ventral RGCs (black boxes). Here again, as for ON cells, RFs were largest at eye-opening, dropping to a minimum at P16 and then increasing again later in development, resulting in no significant difference between P13 and adult. There were no differences between RF diameters sizes between dorsal and ventral cells.

We noticed that the outline of RFs (on the STA spatial plots) seemed blurry at P13, both for ON (Fig 7A, left) and for OFF cells (Fig 7C, left). This blurriness results from a combination of weak STA amplitudes and relatively large RF diameters. To find out how the signal strength is related to the RF diameter at different ages, we plotted the RF diameters of ON (Fig 7E, yellow) and OFF (Fig 7E, blue) RGCs vs the STA amplitudes for all age groups. At P13, there is a wide range of RF diameters (~100-600 μm) but the STA amplitudes are restricted to lower values. The linear regression shows a

significantly negative slope ($p = 0.0045$) for ON, but not for OFF RGCs. At P16, the STA amplitude distribution pattern is similar to P13 but less dispersed and their related RF diameters are restricted to lower values. The linear regression is also significantly negative ($p < 0.0002$) for ON but not for OFF cells at P19 and in adults, STA amplitudes had a much broader distribution than earlier in development while at the same time, RF diameters were more narrowly distributed.

Discussion

In this comprehensive study we have shown that basic firing properties of RGC light responses such as peak firing amplitude, time to peak firing and response duration have a different developmental profile not only in different RGC types but also in dorsal and ventral portions of the retina between eye-opening and adulthood. We also used a novel super-resolution approach for estimating RGC receptive field sizes and polarity across development.

Course of basic response feature development differs between RGC types

At P13, ON RGCs have stronger responses to light than other cell types. As development progresses, these responses become weaker while OFF responses gain strength. We exclude the possibility that the relatively high levels of spontaneous activity (residual of spontaneous waves) could explain these results because peak amplitudes were normalized to baseline activity. Moreover, if spontaneous activity was indeed affecting our measurements, it would equally affect all RGC types, and not just ON cells. An earlier study reported that RGC light responses reach their peak strength around P28, but this study pooled ON , OFF and ON-OFF responses (Tian and Copenhagen, 2001). Pooling our data would yield similar results because of the antagonistic time course of changes in ON and OFF peak amplitudes throughout development (see Fig. 3A). The different maturation time course of ON and OFF peak firing responses may stem from differences in synaptic connectivity and membrane excitability between these cells. A previous study in mouse reported that light-evoked excitatory postsynaptic potentials are larger in ON than in OFF RGCs at P13 (He et al., 2011), but it also stated that both excitatory and inhibitory light-driven synaptic responses are downregulated with age, which cannot explain why we see differences between ON and OFF cells at later ages. An alternative explanation is that the expression

of ionotropic glutamate receptors (AMPA/Kainate and NMDA) differs in ON and OFF RGCs. The NR2A subunit of the NMDA receptor is predominantly found at OFF synapses, while NR2B subunits are preferentially located at ON synapses in rat RGCs (Zhang and Diamond, 2009). However, Stafford et al (2014) found no evidence for a differential localization of the NR2B subunits at ON and OFF synapses in direction selective RGCs until P28 (but no data is available for non-direction selective RGCs) . Another explanation for our observations is that these cells have a different spatial distribution of inhibitory neurotransmitter receptors. A good candidate is the GABAc receptor, expressed presynaptically on bipolar cell axon terminals (Lukasiewicz and Shields, 1998). $GABA_C$ receptors knockout results in stronger and more prolonged spiking activity (Lukasiewicz et al., 2004), similar to our young ON RGCs. Further, $GABA_C$-receptor mediated inhibition affects the regulation of glutamatergic synaptic transmission at the ON but not at the OFF bipolar-RGC synapse (Sagdullaev et al., 2006). But Schubert et al., (2008) showed that ON and OFF bipolar cell spontaneous inhibitory postsynaptic currents (IPSCs) are relatively similar at P12. However, the nature of light-evoked GABAergic inputs onto developing mouse bipolar cells, and how it differs for different RGC types remains to be determined (but see He et al., 2011).

The response durations of ON and OFF RGCs in our study showed a similar antagonistic behavior like for the peak amplitudes (Fig. 3A) whereas the decrease is much stronger in ON than in OFF RGCs and a massive drop occurs during the fourth postnatal week (Fig. 3A). $GABA_C$ receptors consists of ρ subunits and the ρ1 subunit expression peaks around P9 (start P6) and ρ2, around P15 (start P9) (Greka et al., 2000). The difference in the timing of peak expression of these subunits may explain the differences we observe between ON and OFF RGCs,

Response latencies did not exhibit conspicuous differences between different RGC types from eye opening to adulthood and the changes we observed most likely reflect ongoing activity-mediated refinement of the bipolar-RGC synapse (Tootle, 1993; Myhr et al., 2001; Tian and Copenhagen, 2001; Wang et al., 2001; He et al., 2011; Tian, 2011). Functional and morphological refinement result in the establishment of distinct functional differences between RGC types, as summarized by the Fano factor measure.

Dorsal and ventral RGCs have a different developmental functional profile

In mouse, S-opsins are co-expressed with M-opsins. Moreover, S-opsin in the "true" S-cones (Haverkamp, 2005) exhibit peak excitation around 360 nm (Jacobs et al., 1991; Wang et al., 2011). To stimulate retinas in our study, we have used a broad spectrum white light composed of red, green and blue LED lights (~420 – 660 nm) but not UV light. Therefore it is highly unlikely that we were able to stimulate pure S-cones. We are aware that under these conditions, dorsal RGCs have an advantage because our white light source is biased towards activation of M-opsin, which is more prevalent in the dorsal retina. However, we have used exactly the same light spectrum for all retinas and our aim is to undertake a systematic comparative study of the ontogeny of light-driven responses in different RGC types located in ventral versus dorsal retinal areas from eye opening to adulthood. In addition, our results do not demonstrate a general increase of response strength in the dorsal side *per se*. Further, the maximum light intensity (white light: 20 cd/m^2) in our experiments was set to co-activate rods and cones. Therefore rod-mediated (rhodopsin) responses are not saturated in our recordings (Naarendorp et al., 2010), and they probably reflect a large proportion of our recordings.

S- and M-opsins are expressed before eye-opening, respectively from ~P1 and ~P8 (Szél et al., 1996; Applebury et al., 2000). Therefore we can reasonably assume that both S- and M-opsin gradients are already fully established shortly after eye opening, when we sampled the earliest light responses, and differences in opsin expression are unlikely to explain our findings. Moreover, even though a bias in M-opsin at P13 could potentially explain the stronger responses we recorded at that age, it cannot be responsible for the results we found at later developmental stages, including a switch to stronger ventral responses at low contrast levels in the adult retina. Interestingly, we found that low contrast full fields flashed to the dorsal side do not evoke strong light responses in adult retinas, while these responses are significantly stronger at P13, which cannot be explained by a bias in M-opsin activation. Stronger responses in the dorsal retina at the onset of visual experience is not an unreasonable possibility from an ecological and evolutionary point of view because at that age, pups are still gathered in the nest, near the mother, with no ecological need to look skywards, but they rather concentrate on the nest scenery, using dorsal retinal vision. In the ensuing week, retinal circuits keep developing and refining, leading to maturation of the ventral circuitry as well.

445

446 **Mapping RFs with shifted white noise**

447 Presenting white noise checkerboard images and performing a post hoc reverse correlation is now a
448 standard approach to estimate RGC RF centers (Rieke et al., 1997; Chichilnisky, 2001). However, the
449 technique is challenging in very young retinas because of high levels of spontaneous activity and the
450 weak sensitivity to light in young RGCs immediately after eye opening. The problem can be alleviated
451 by increasing the number of trials and/or the pixel size without compromising the minimum resolution
452 for reliable RF estimation (Schwartz et al., 2006; Cantrell et al., 2010; Koehler et al., 2011). Here we
453 introduce a novel powerful approach, the SWN, which uses big checkerboard pixels (hence evoking
454 strong responses) randomly shifted in space and time by a fraction of the pixel size, yielding better
455 resolution. SWN images are uncorrelated across time and the bias introduced by the correlation in space
456 due to finite pixel size is negligible.
457 Using that SWN approach, we have shown that RFs in ON RGCs are significantly larger at P13 than
458 later in development, and that in OFF cells, RFs are similar in size at P13 and in adults, with a temporary
459 drop during the third postnatal week. Previous studies which used conventional checkerboard images
460 present a different developmental picture. Koehler et al (2011) showed that ON and OFF RFs are
461 smaller in adults than immediately after eye-opening whereas Cantrell et al. (2010) stated that OFF, but
462 not ON RFs expand between P15-18 and that there is a significant difference for ON, but not for OFF
463 cells between P18-25. This demonstrates that different white noise approaches can yield different
464 results. Additional factors such as mean luminance, adaptational state, recording length and stimulus
465 refresh rate may account for these differences, and results should therefore be interpreted with caution.
466 We also looked at developmental changes in the signal (STA) strength. Cantrell et al. (2010) observed
467 that increased signal strength is associated with smaller rather than larger RFs. We found a similar
468 behavior only in ON RGCs at P13-16 (negative slope for the linear regression). In our hands, the STA
469 strength increases later in development, probably reflecting the ongoing strengthening and refinement
470 of the bipolar–RGC synapse.

471

472

473 **References**

474 Applebury ML, Antoch MP, Baxter LC, Chun LL, Falk JD, Farhangfar F, Kage K, Krzystolik MG,
475 Lyass L a, Robbins JT (2000) The murine cone photoreceptor: a single cone type expresses both
476 S and M opsins with retinal spatial patterning. Neuron 27:513–523.

477 Baden T, Schubert T, Chang L, Wei T, Zaichuk M, Wissinger B, Euler T (2013) A tale of two retinal
478 domains: Near-Optimal sampling of achromatic contrasts in natural scenes through asymmetric
479 photoreceptor distribution. Neuron 80:1206–1217 Available at:
480 http://dx.doi.org/10.1016/j.neuron.2013.09.030.

481 Berdondini L, Imfeld K, Maccione A, Tedesco M, Neukom S, Koudelka-Hep M, Martinoia S (2009)
482 Active pixel sensor array for high spatio-temporal resolution electrophysiological recordings
483 from single cell to large scale neuronal networks. Lab Chip 9:2644 Available at:
484 http://xlink.rsc.org/?DOI=b907394a.

485 Bleckert A, Schwartz GW, Turner MH, Rieke F, Wong ROL (2014) Visual space is represented by
486 nonmatching topographies of distinct mouse retinal ganglion cell types. Curr Biol 24:310–315
487 Available at: http://dx.doi.org/10.1016/j.cub.2013.12.020.

488 Cantrell DR, Cang J, Troy JB, Liu X (2010) Non-Centered Spike-Triggered Covariance Analysis
489 Reveals Neurotrophin-3 as a Developmental Regulator of Receptive Field Properties of ON-
490 OFF Retinal Ganglion Cells. PLoS Comput Biol 6:e1000967 Available at:
491 http://dx.plos.org/10.1371/journal.pcbi.1000967.

492 Carcieri SM, Jacobs AL, Nirenberg S (2003) Classification of retinal ganglion cells: a statistical
493 approach. J Neurophysiol 90:1704–1713.

494 Chang L, Breuninger T, Euler T (2013) Chromatic Coding from Cone-type Unselective Circuits in the
495 Mouse Retina. Neuron 77:559–571 Available at:
496 http://linkinghub.elsevier.com/retrieve/pii/S0896627312011221.

497 Chen H, Liu X, Tian N (2014) Subtype-dependent postnatal development of direction- and
498 orientation-selective retinal ganglion cells in mice. J Neurophysiol 112:2092–2101 Available at:
499 http://jn.physiology.org/cgi/doi/10.1152/jn.00320.2014.

500 Chichilnisky EJ (2001) A simple white noise analysis of neuronal light responses. Network 12:199–

213 Available at: http://www.ncbi.nlm.nih.gov/pubmed/11405422\nhttp://informahealthcare.com/doi/abs/10.1080/net.12.2.199.213.

Ekesten B, Gouras P (2005) Cone and rod inputs to murine retinal ganglion cells: evidence of cone opsin specific channels. Vis Neurosci 22:893–903.

Elstrott J, Anishchenko A, Greschner M, Sher A, Litke AM, Chichilnisky EJ, Feller MB (2008) Direction Selectivity in the Retina Is Established Independent of Visual Experience and Cholinergic Retinal Waves. Neuron 58:499–506 Available at: http://linkinghub.elsevier.com/retrieve/pii/S0896627308002596.

Greka A, Lipton S, Zhang D (2000) Expression of GABA C receptor r1 and r2 subunits during development of the mouse retina. 12:3575–3582.

Haverkamp S (2005) The Primordial, Blue-Cone Color System of the Mouse Retina. J Neurosci 25:5438–5445 Available at: http://www.jneurosci.org/cgi/doi/10.1523/JNEUROSCI.1117-05.2005.

He Q, Wang P, Tian N (2011) Light-evoked synaptic activity of retinal ganglion and amacrine cells is regulated in developing mouse retina. Eur J Neurosci 33:36–48 Available at: http://www.ncbi.nlm.nih.gov/pubmed/21091802\nhttp://www.pubmedcentral.nih.gov/articlerender.fcgi?artid=3070459&tool=pmcentrez&rendertype=abstract.

Jacobs GH, Neitz J, Deegan JF (1991) Retinal receptors in rodents maximally sensitive to ultraviolet light. Nature 353:655–656.

Koehler CL, Akimov NP, Rentería RC (2011) Receptive field center size decreases and firing properties mature in ON and OFF retinal ganglion cells after eye opening in the mouse. J Neurophysiol 106:895–904.

Lukasiewicz PD, Eggers ED, Sagdullaev BT, McCall MA (2004) GABAC receptor-mediated inhibition in the retina. Vision Res 44:3289–3296 Available at: http://linkinghub.elsevier.com/retrieve/pii/S0042698904003608.

Lukasiewicz PD, Shields CR (1998) A diversity of GABA receptors in the retina. Semin Cell Dev Biol 9:293–299 Available at: http://www.ncbi.nlm.nih.gov/pubmed/9665865.

529 Lukáts Á, Szabó a., Röhlich P, Vígh B, Szél Á (2005) Photopigment coexpression in mammals:
530 Comparative and developmental aspects. Histol Histopathol 20:551–574.
531 Maccione A, Hennig MH, Gandolfo M, Muthmann O, van Coppenhagen J, Eglen SJ, Berdondini L,
532 Sernagor E (2014) Following the ontogeny of retinal waves: pan-retinal recordings of population
533 dynamics in the neonatal mouse. J Physiol 592:1545–1563 Available at:
534 http://www.ncbi.nlm.nih.gov/pubmed/24366261.
535 Masland RH (1977) Maturation of function in the developing rabbit retina. J Comp Neurol 175:275–
536 286 Available at: http://www.ncbi.nlm.nih.gov/pubmed/903424.
537 Muthmann J-O, Amin H, Sernagor E, Maccione A, Panas D, Berdondini L, Bhalla US, Hennig MH
538 (2015) Spike Detection for Large Neural Populations Using High Density Multielectrode
539 Arrays. Front Neuroinform 9:1–21 Available at:
540 http://journal.frontiersin.org/Article/10.3389/fninf.2015.00028/abstract.
541 Myhr KL, Lukasiewicz PD, Wong RO (2001) Mechanisms underlying developmental changes in the
542 firing patterns of ON and OFF retinal ganglion cells during refinement of their central
543 projections. J Neurosci 21:8664–8671 Available at:
544 http://www.ncbi.nlm.nih.gov/pubmed/11606654.
545 Naarendorp F, Esdaille TM, Banden SM, Andrews-Labenski J, Gross OP, Pugh EN (2010) Dark
546 Light, Rod Saturation, and the Absolute and Incremental Sensitivity of Mouse Cone Vision. J
547 Neurosci 30:12495–12507 Available at:
548 http://www.jneurosci.org/cgi/doi/10.1523/JNEUROSCI.2186-10.2010.
549 Pamplona D, Hilgen G, Cessac B, Sernagor E, Kornprobst P (2015) A super-resolution approach for
550 receptive fields estimation of neuronal ensembles. BMC Neurosci 16.
551 Peichl L (2005) Diversity of mammalian photoreceptor properties: Adaptations to habitat and
552 lifestyle? Anat Rec - Part A Discov Mol Cell Evol Biol 287:1001–1012.
553 Rieke F, Warland D, de Ruyter van Steveninck RR, Bialek W (1997) Spikes: Exploring the neural
554 code. Cambridge, MA: MIT Press.
555 Röhlich P, van Veen T, Szél Á (1994) Two different visual pigments in one retinal cone cell. Neuron
556 13:1159–1166 Available at:

http://www.sciencedirect.com/science/article/pii/0896627394900531.

Sagdullaev BT, McCall MA, Lukasiewicz PD (2006) Presynaptic Inhibition Modulates Spillover, Creating Distinct Dynamic Response Ranges of Sensory Output. Neuron 50:923–935 Available at: http://linkinghub.elsevier.com/retrieve/pii/S0896627306003825.

Schubert T, Kerschensteiner D, Eggers ED, Misgeld T, Kerschensteiner M, Lichtman JW, Lukasiewicz PD, Wong ROL (2008) Development of Presynaptic Inhibition Onto Retinal Bipolar Cell Axon Terminals Is Subclass-Specific. J Neurophysiol 100:304–316 Available at: http://jn.physiology.org/cgi/doi/10.1152/jn.90202.2008.

Schwartz O, Pillow JW, Rust NC, Simoncelli EP (2006) Spike-triggered neural characterization. J Vis 6:484–507 Available at: http://www.ncbi.nlm.nih.gov/pubmed/16889482.

Sernagor E, Chalupa LM (2006) Emergence of light responses. In: Retinal Development (Sernagor E, Eglen S., Harris B, Wong ROL, eds), pp 288–304. Cambridge University Press.

Sernagor E, Grzywacz NM (1995) Emergence of complex receptive field properties of ganglion cells in the developing turtle retina. J Neurophysiol 73:1355–1364 Available at: http://www.ncbi.nlm.nih.gov/pubmed/7643153.

Stafford BK, Park SJH, Wong KY, Demb JB (2014) Developmental Changes in NMDA Receptor Subunit Composition at ON and OFF Bipolar Cell Synapses onto Direction-Selective Retinal Ganglion Cells. J Neurosci 34:1942–1948 Available at: http://www.jneurosci.org/cgi/doi/10.1523/JNEUROSCI.4461-13.2014.

Szel a., Rohlich P, Caffe a. R, Juliusson B, Aguirre G, Van Veen T (1992) Unique topographic separation of two spectral classes of cones in the mouse retina. J Comp Neurol 325:327–342.

Szél Á, Röhlich P, Caffé AR, van Veen T (1996) Distribution of cone photoreceptors in the mammalian retina. Microsc Res Tech 35:445–462 Available at: http://dx.doi.org/10.1002/(SICI)1097-0029(19961215)35:6<445::AID-JEMT4>3.0.CO;2-H.

Tian N (2011) Developmental mechanisms that regulate retinal ganglion cell dendritic morphology. Dev Neurobiol 71:1297–1309 Available at: http://doi.wiley.com/10.1002/dneu.20900.

Tian N, Copenhagen DR (2001) Visual deprivation alters development of synaptic function in inner retina after eye opening. Neuron 32:439–449.

585 Tian N, Copenhagen DR (2003) Visual stimulation is required for refinement on ON and OFF
586 pathways in postnatal retina. Neuron 39:85–96.
587 Tootle JS (1993) Early postnatal development of visual function in ganglion cells of the cat retina. J
588 Neurophysiol 69:1645–1660.
589 Wang Y V., Weick M, Demb JB (2011) Spectral and Temporal Sensitivity of Cone-Mediated
590 Responses in Mouse Retinal Ganglion Cells. J Neurosci 31:7670–7681 Available at:
591 http://www.jneurosci.org/cgi/doi/10.1523/JNEUROSCI.0629-11.2011.
592 Wang GY, Liets LC, Chalupa LM (2001) Unique functional properties of on and off pathways in the
593 developing mammalian retina. J Neurosci 21:4310–4317 Available at:
594 http://www.ncbi.nlm.nih.gov/pubmed/11404416.
595 Wei W, Elstrott J, Feller MB (2010) Two-photon targeted recording of GFP-expressing neurons for
596 light responses and live-cell imaging in the mouse retina. Nat Protoc 5:1347–1352 Available at:
597 http://dx.doi.org/10.1038/nprot.2010.106 [Accessed November 26, 2015].
598 Yin L, Smith RG, Sterling P, Brainard DH (2009) Physiology and morphology of color-opponent
599 ganglion cells in a retina expressing a dual gradient of S and M opsins. J Neurosci 29:2706–
600 2724.
601 Zhang J, Diamond JS (2009) Subunit- and pathway-specific localization of NMDA receptors and
602 scaffolding proteins at ganglion cell synapses in rat retina. J Neurosci 29:4274–4286.
603 Zhang Y, Kim I-J, Sanes JR, Meister M (2012) The most numerous ganglion cell type of the mouse
604 retina is a selective feature detector. Proc Natl Acad Sci 109:E2391–E2398 Available at:
605 http://www.pnas.org/cgi/doi/10.1073/pnas.1211547109.
606
607 Baden T, Schubert T, Chang L, Wei T, Zaichuk M, Wissinger B, Euler T (2013) A tale of two retinal
608 domains: Near-Optimal sampling of achromatic contrasts in natural scenes through asymmetric
609 photoreceptor distribution. Neuron 80:1206–1217 Available at:
610 http://dx.doi.org/10.1016/j.neuron.2013.09.030.
611 Berdondini L, Imfeld K, Maccione A, Tedesco M, Neukom S, Koudelka-Hep M, Martinoia S (2009)
612 Active pixel sensor array for high spatio-temporal resolution electrophysiological recordings

613 from single cell to large scale neuronal networks. Lab Chip 9:2644 Available at:
614 http://xlink.rsc.org/?DOI=b907394a.
615 Bleckert A, Schwartz GW, Turner MH, Rieke F, Wong ROL (2014) Visual space is represented by
616 nonmatching topographies of distinct mouse retinal ganglion cell types. Curr Biol 24:310–315
617 Available at: http://dx.doi.org/10.1016/j.cub.2013.12.020.
618 Cantrell DR, Cang J, Troy JB, Liu X (2010) Non-Centered Spike-Triggered Covariance Analysis
619 Reveals Neurotrophin-3 as a Developmental Regulator of Receptive Field Properties of ON-
620 OFF Retinal Ganglion Cells. PLoS Comput Biol 6:e1000967 Available at:
621 http://dx.plos.org/10.1371/journal.pcbi.1000967.
622 Carcieri SM, Jacobs AL, Nirenberg S (2003) Classification of retinal ganglion cells: a statistical
623 approach. J Neurophysiol 90:1704–1713.
624 Chang L, Breuninger T, Euler T (2013) Chromatic Coding from Cone-type Unselective Circuits in the
625 Mouse Retina. Neuron 77:559–571 Available at:
626 http://linkinghub.elsevier.com/retrieve/pii/S0896627312011221.
627 Chen H, Liu X, Tian N (2014) Subtype-dependent postnatal development of direction- and
628 orientation-selective retinal ganglion cells in mice. J Neurophysiol 112:2092–2101 Available at:
629 http://jn.physiology.org/cgi/doi/10.1152/jn.00320.2014.
630 Chichilnisky EJ (2001) A simple white noise analysis of neuronal light responses. Network 12:199–
631 213 Available at:
632 http://www.ncbi.nlm.nih.gov/pubmed/11405422\nhttp://informahealthcare.com/doi/abs/10.1080/
633 net.12.2.199.213.
634 Ekesten B, Gouras P (2005) Cone and rod inputs to murine retinal ganglion cells: evidence of cone
635 opsin specific channels. Vis Neurosci 22:893–903.
636 Elstrott J, Anishchenko A, Greschner M, Sher A, Litke AM, Chichilnisky EJ, Feller MB (2008)
637 Direction Selectivity in the Retina Is Established Independent of Visual Experience and
638 Cholinergic Retinal Waves. Neuron 58:499–506 Available at:
639 http://linkinghub.elsevier.com/retrieve/pii/S0896627308002596.
640 Greka A, Lipton S, Zhang D (2000) Expression of GABA C receptor r1 and r2 subunits during

development of the mouse retina. 12:3575–3582.

Haverkamp S (2005) The Primordial, Blue-Cone Color System of the Mouse Retina. J Neurosci 25:5438–5445 Available at: http://www.jneurosci.org/cgi/doi/10.1523/JNEUROSCI.1117-05.2005.

He Q, Wang P, Tian N (2011) Light-evoked synaptic activity of retinal ganglion and amacrine cells is regulated in developing mouse retina. Eur J Neurosci 33:36–48 Available at: http://www.ncbi.nlm.nih.gov/pubmed/21091802\nhttp://www.pubmedcentral.nih.gov/articlerender.fcgi?artid=3070459&tool=pmcentrez&rendertype=abstract.

Jacobs GH, Neitz J, Deegan JF (1991) Retinal receptors in rodents maximally sensitive to ultraviolet light. Nature 353:655–656.

Koehler CL, Akimov NP, Rentería RC (2011) Receptive field center size decreases and firing properties mature in ON and OFF retinal ganglion cells after eye opening in the mouse. J Neurophysiol 106:895–904.

Lukasiewicz PD, Eggers ED, Sagdullaev BT, McCall MA (2004) GABAC receptor-mediated inhibition in the retina. Vision Res 44:3289–3296 Available at: http://linkinghub.elsevier.com/retrieve/pii/S0042698904003608.

Lukasiewicz PD, Shields CR (1998) A diversity of GABA receptors in the retina. Semin Cell Dev Biol 9:293–299 Available at: http://www.ncbi.nlm.nih.gov/pubmed/9665865.

Lukáts Á, Szabó a., Röhlich P, Vígh B, Szél Á (2005) Photopigment coexpression in mammals: Comparative and developmental aspects. Histol Histopathol 20:551–574.

Maccione A, Hennig MH, Gandolfo M, Muthmann O, van Coppenhagen J, Eglen SJ, Berdondini L, Sernagor E (2014) Following the ontogeny of retinal waves: pan-retinal recordings of population dynamics in the neonatal mouse. J Physiol 592:1545–1563 Available at: http://www.ncbi.nlm.nih.gov/pubmed/24366261.

Masland RH (1977) Maturation of function in the developing rabbit retina. J Comp Neurol 175:275–286 Available at: http://www.ncbi.nlm.nih.gov/pubmed/903424.

Muthmann J-O, Amin H, Sernagor E, Maccione A, Panas D, Berdondini L, Bhalla US, Hennig MH (2015) Spike Detection for Large Neural Populations Using High Density Multielectrode

669 Arrays. Front Neuroinform 9:1–21 Available at:
670 http://journal.frontiersin.org/Article/10.3389/fninf.2015.00028/abstract.
671 Myhr KL, Lukasiewicz PD, Wong RO (2001) Mechanisms underlying developmental changes in the
672 firing patterns of ON and OFF retinal ganglion cells during refinement of their central
673 projections. J Neurosci 21:8664–8671 Available at:
674 http://www.ncbi.nlm.nih.gov/pubmed/11606654.
675 Naarendorp F, Esdaille TM, Banden SM, Andrews-Labenski J, Gross OP, Pugh EN (2010) Dark
676 Light, Rod Saturation, and the Absolute and Incremental Sensitivity of Mouse Cone Vision. J
677 Neurosci 30:12495–12507 Available at:
678 http://www.jneurosci.org/cgi/doi/10.1523/JNEUROSCI.2186-10.2010.
679 Peichl L (2005) Diversity of mammalian photoreceptor properties: Adaptations to habitat and
680 lifestyle? Anat Rec - Part A Discov Mol Cell Evol Biol 287:1001–1012.
681 Rieke F, Warland D, de Ruyter van Steveninck RR, Bialek W (1997) Spikes: Exploring the neural
682 code. Cambridge, MA: MIT Press.
683 Röhlich P, van Veen T, Szél Á (1994) Two different visual pigments in one retinal cone cell. Neuron
684 13:1159–1166 Available at:
685 http://www.sciencedirect.com/science/article/pii/0896627394900531.
686 Sagdullaev BT, McCall MA, Lukasiewicz PD (2006) Presynaptic Inhibition Modulates Spillover,
687 Creating Distinct Dynamic Response Ranges of Sensory Output. Neuron 50:923–935 Available
688 at: http://linkinghub.elsevier.com/retrieve/pii/S0896627306003825.
689 Schubert T, Kerschensteiner D, Eggers ED, Misgeld T, Kerschensteiner M, Lichtman JW,
690 Lukasiewicz PD, Wong ROL (2008) Development of Presynaptic Inhibition Onto Retinal
691 Bipolar Cell Axon Terminals Is Subclass-Specific. J Neurophysiol 100:304–316 Available at:
692 http://jn.physiology.org/cgi/doi/10.1152/jn.90202.2008.
693 Schwartz O, Pillow JW, Rust NC, Simoncelli EP (2006) Spike-triggered neural characterization. J Vis
694 6:484–507 Available at: http://www.ncbi.nlm.nih.gov/pubmed/16889482.
695 Sernagor E, Chalupa LM (2006) Emergence of light responses. In: Retinal Development (Sernagor E,
696 Eglen S., Harris B, Wong ROL, eds), pp 288–304. Cambridge University Press.

Sernagor E, Grzywacz NM (1995) Emergence of complex receptive field properties of ganglion cells in the developing turtle retina. J Neurophysiol 73:1355–1364 Available at: http://www.ncbi.nlm.nih.gov/pubmed/7643153.

Stafford BK, Park SJH, Wong KY, Demb JB (2014) Developmental Changes in NMDA Receptor Subunit Composition at ON and OFF Bipolar Cell Synapses onto Direction-Selective Retinal Ganglion Cells. J Neurosci 34:1942–1948 Available at: http://www.jneurosci.org/cgi/doi/10.1523/JNEUROSCI.4461-13.2014.

Szel a., Rohlich P, Caffe a. R, Juliusson B, Aguirre G, Van Veen T (1992) Unique topographic separation of two spectral classes of cones in the mouse retina. J Comp Neurol 325:327–342.

Szél Á, Röhlich P, Caffé AR, van Veen T (1996) Distribution of cone photoreceptors in the mammalian retina. Microsc Res Tech 35:445–462 Available at: http://dx.doi.org/10.1002/(SICI)1097-0029(19961215)35:6<445::AID-JEMT4>3.0.CO;2-H.

Tian N (2011) Developmental mechanisms that regulate retinal ganglion cell dendritic morphology. Dev Neurobiol 71:1297–1309 Available at: http://doi.wiley.com/10.1002/dneu.20900.

Tian N, Copenhagen DR (2001) Visual deprivation alters development of synaptic function in inner retina after eye opening. Neuron 32:439–449.

Tian N, Copenhagen DR (2003) Visual stimulation is required for refinement on ON and OFF pathways in postnatal retina. Neuron 39:85–96.

Tootle JS (1993) Early postnatal development of visual function in ganglion cells of the cat retina. J Neurophysiol 69:1645–1660.

Wang GY, Liets LC, Chalupa LM (2001) Unique functional properties of on and off pathways in the developing mammalian retina. J Neurosci 21:4310–4317 Available at: http://www.ncbi.nlm.nih.gov/pubmed/11404416.

Wang Y V., Weick M, Demb JB (2011) Spectral and Temporal Sensitivity of Cone-Mediated Responses in Mouse Retinal Ganglion Cells. J Neurosci 31:7670–7681 Available at: http://www.jneurosci.org/cgi/doi/10.1523/JNEUROSCI.0629-11.2011.

Wei W, Elstrott J, Feller MB (2010) Two-photon targeted recording of GFP-expressing neurons for light responses and live-cell imaging in the mouse retina. Nat Protoc 5:1347–1352 Available at:

http://dx.doi.org/10.1038/nprot.2010.106 [Accessed November 26, 2015].

Yin L, Smith RG, Sterling P, Brainard DH (2009) Physiology and morphology of color-opponent ganglion cells in a retina expressing a dual gradient of S and M opsins. J Neurosci 29:2706–2724.

Zhang J, Diamond JS (2009) Subunit- and pathway-specific localization of NMDA receptors and scaffolding proteins at ganglion cell synapses in rat retina. J Neurosci 29:4274–4286.

Zhang Y, Kim I-J, Sanes JR, Meister M (2012) The most numerous ganglion cell type of the mouse retina is a selective feature detector. Proc Natl Acad Sci 109:E2391–E2398 Available at: http://www.pnas.org/cgi/doi/10.1073/pnas.1211547109.

Legends

Table 1

Numbers (n) of dorsal and ventral ON, OFF and ON-OFF retinal ganglion cells for the different age groups

Figure 1

Response parameter calculations and shifted white noise paradigm. A) Top row is showing a spike raster of a full field stimulus (30 trials, 2 sec on, 2 sec off) where each dot is representing a spike, bottom row shows the averaged trials (see methods, converted to Spikes/Sec). Baseline firing rate was estimated by looking at each unit's activity (Spikes/Sec) before stimuli were presented (>30 sec). *A1* (Spikes/Sec)

753 is the first maximum peak (measured from each unit's baseline) after stimulus onset and *A2* the first
754 maximum peak after stimulus offset. *T2P1* (ms) is the time from stimulus onset to *A1*, *T2P2* the time
755 from stimulus offset, respectively. *RD1* (ms) is the time, so-called response duration, after *A1* where
756 the response is still above *A1/e*. *RD2* is the response duration after *A2* to *A2/e*. B) Top is showing the
757 standard white noise paradigm with static located pixels and the resulting resolution (*P*) of the spatial
758 STA profile. Bottom is showing the shifted white noise paradigm but with shifted (*S*) pixel location.
759 This results in a much finer resolution (*P/S*) for the spatial STA profile.
760
761 **Figure 2**
762 Activity maps and spike raster plots of a P13 and a P38 retina. A) The *Log* spike count (full field
763 stimulus experiment) for each channel from a P13 (top) and a P38 (bottom) retina is pseudo color-coded
764 and plotted according to electrode coordinates (64 x 64 array). This results in a visualization of the
765 retina outline and gives an overall estimation of the number of active channels. B) Spike raster plots
766 from the same P13 and P38 experiment used for A) but after spike sorting. Each dot is representing a
767 spike in an alternating full field stimulus experiment and dots are color-coded: green = ON RGCs, red
768 = OFF RGCs, blue = ON-OFF and the raster plots are divided into dorsal and ventral RGCs. The binned
769 (25 ms) average response (Spikes/Sec) of all RGCs is plotted below the raster plots and with colors
770 matching the corresponding spike dots.
771
772 **Figure 3**
773 Response properties and trial variability of different RGC types from P13 to P29/P38. A, B, C:
774 respectively illustrate Peak Amplitude (*A1, A2*), Time to Peak (*T2P1, T2P2*) and Response Duration
775 (*RD1, RD2*) for dorsal (green) and ventral (blue) ON (left), OFF (middle) and ON-OFF (right) RGCs
776 for each age group (mean values with 95% confidence interval, n = Table 1). For ON-OFF cells the
777 light on- and offset values were calculated as ON-OFF 1 (solid line) and ON-OFF 2 (dotted line),
778 respectively. Significance: * = $p < 0.05$; ** = $p < 0.01$; *** = $p < 0.001$. Dark asterisks are for onset
779 values, grey asterisks for offset values. B) Plots representing the average Fano factor (+ SEM (shadow),

n = Table 1) for the different RGC types, calculated in 25 ms bins and color coded according to age groups.

Figure 4

Dorsal-ventral gradient of peak amplitudes to different contrasts after eye-opening. A) ON peak amplitudes (*A1* in Spikes/Sec) for three different full field contrasts (0.41, 0.53, 0.62) from a single P13 retina are plotted in pseudo colors according to firing strength and electrode position. For visualization, the individual x,y electrode position for the peak values was slightly randomly shifted (+/- 0.25) because after spike sorting multiple RGC units are assigned to the same electrode position. B) Mean peak response amplitudes to different full field Michelson contrasts (0.19, 0.41, 0.53, 0.62, 0.67) for ON (top), OFF (middle) and ON-OFF (bottom) RGC types for all age groups (ascending from left to right) with respect to their dorsal (green) or ventral (blue) location. All plot conventions are like for Figure 3A.

Figure 5

Dorsal-ventral differences for the time to peak values at lower contrast in the adult retina. A) OFF RGC color-coded response times to peak (*T2P2* in ms) from a single P38 at three different full field contrasts (0.19, 0.53, 0.7) plotted according to their electrode position. B) Mean times to peak plotted for the different full field Michelson contrasts (x axis, 0.19, 0.41, 0.53, 0.62, 0.67) for ON (top), OFF (middle) and ON-OFF (bottom) RGC types and all age groups. All plot conventions are like for Figure 3A.

Figure 6

Responses to light are more sustained for all dorsal RGC types than for their ventral counterparts. A) The ON RGC response duration times (*RD1* in ms) from a single P13 retina of three different full field contrasts (0.19, 0.62, 0.7) were pseudo colour-coded plotted according to their electrode position. B) The mean response duration times to different full field Michelson contrasts (x axis, 0.19, 0.41, 0.53, 0.62, 0.67) for ON (top), OFF (middle) and ON-OFF (bottom) RGC types and all age groups. All plot conventions are like for Figure 3A.

Figure 7

Shifted White Noise used to study the development of RGC RF central areas. A, C: STA time courses (top) and spatial profiles with the fitted RFs (bottom) for selected example RF central areas from ON (A) and OFF (C) RGCs from all 4 age groups. B, D: box plots (whiskers: 10-90 percentile, mean indicated by + symbol) of RF diameters for ON (B, yellow) and OFF (D, blue) RGCs from all retinal areas. RF diameters are also shown separately for dorsal and ventral located RGCs (black). E: RF diameters of ON (yellow) and OFF (blue) RGCs plotted against their corresponding STA amplitude for all 4 age groups. Blue (OFF RGCs) and yellow (ON RGCs) represent linear regressions to estimate the slope of the corresponding data distribution. Significance: * = $p < 0.05$; ** = $p < 0.01$; *** = $p < 0.001$.

Illustrations and Tables

Table 1

		P13 (4 retinas)	P16/P17 (4 retinas)	P19 (3 retinas)	P29/P38 (4 retinas)
ON	Dorsal	1386	540	470	1594
	Ventral	460	1278	523	835
	Total	**1846**	**1818**	**993**	**2429**
OFF	Dorsal	576	463	462	1401

	Ventral	286	729	388	435
	Total	**862**	**1192**	**850**	**1836**
ON-OFF	Dorsal	1017	481	702	1101
	Ventral	458	913	665	445
	Total	**1475**	**1394**	**1367**	**1546**

Figure 1

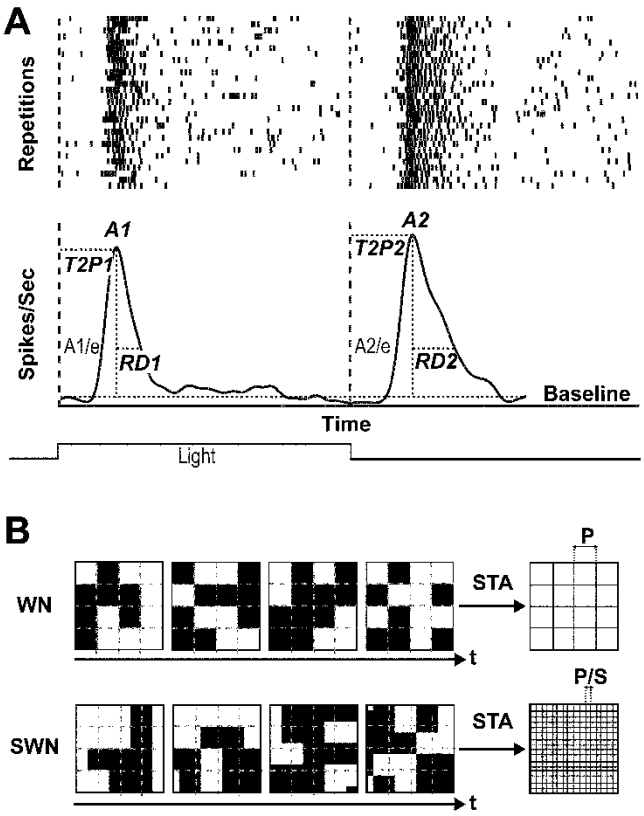

843

844 **Figure 2**

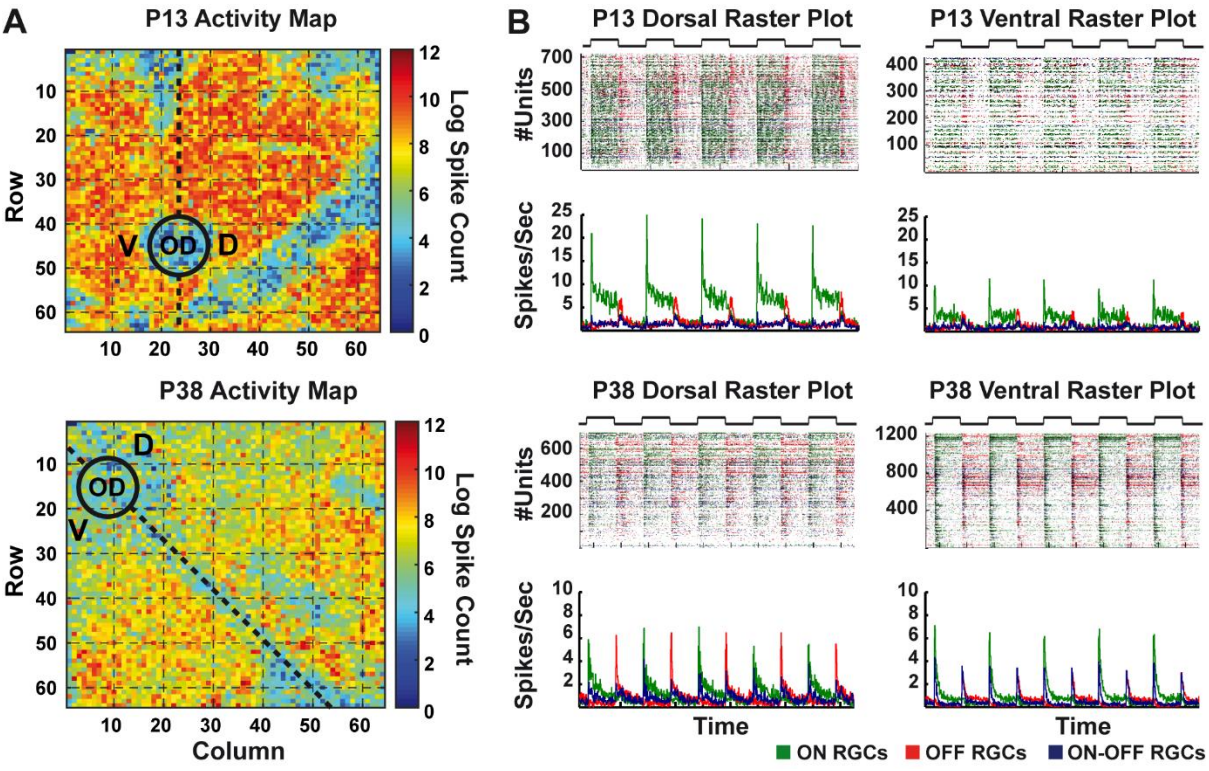

845

846

847 **Figure 3**

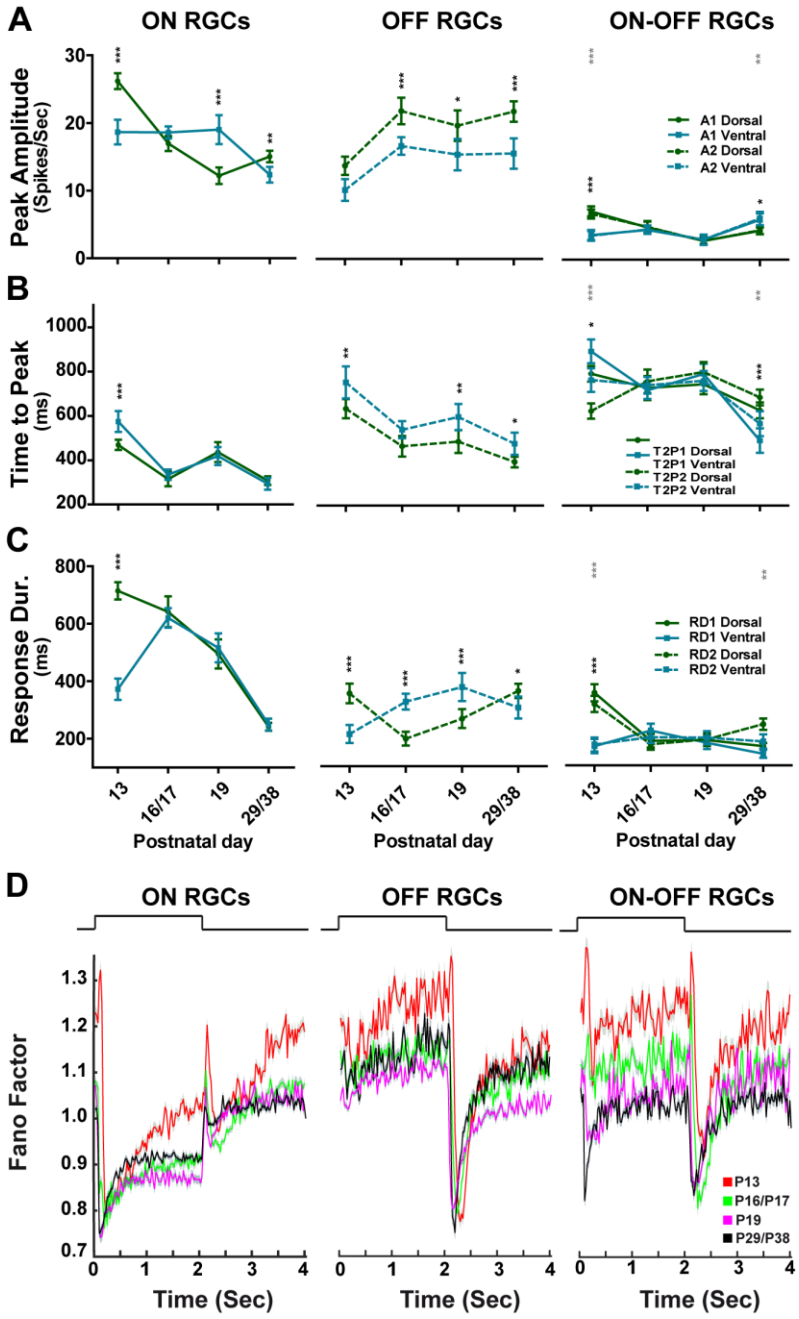

Figure 4

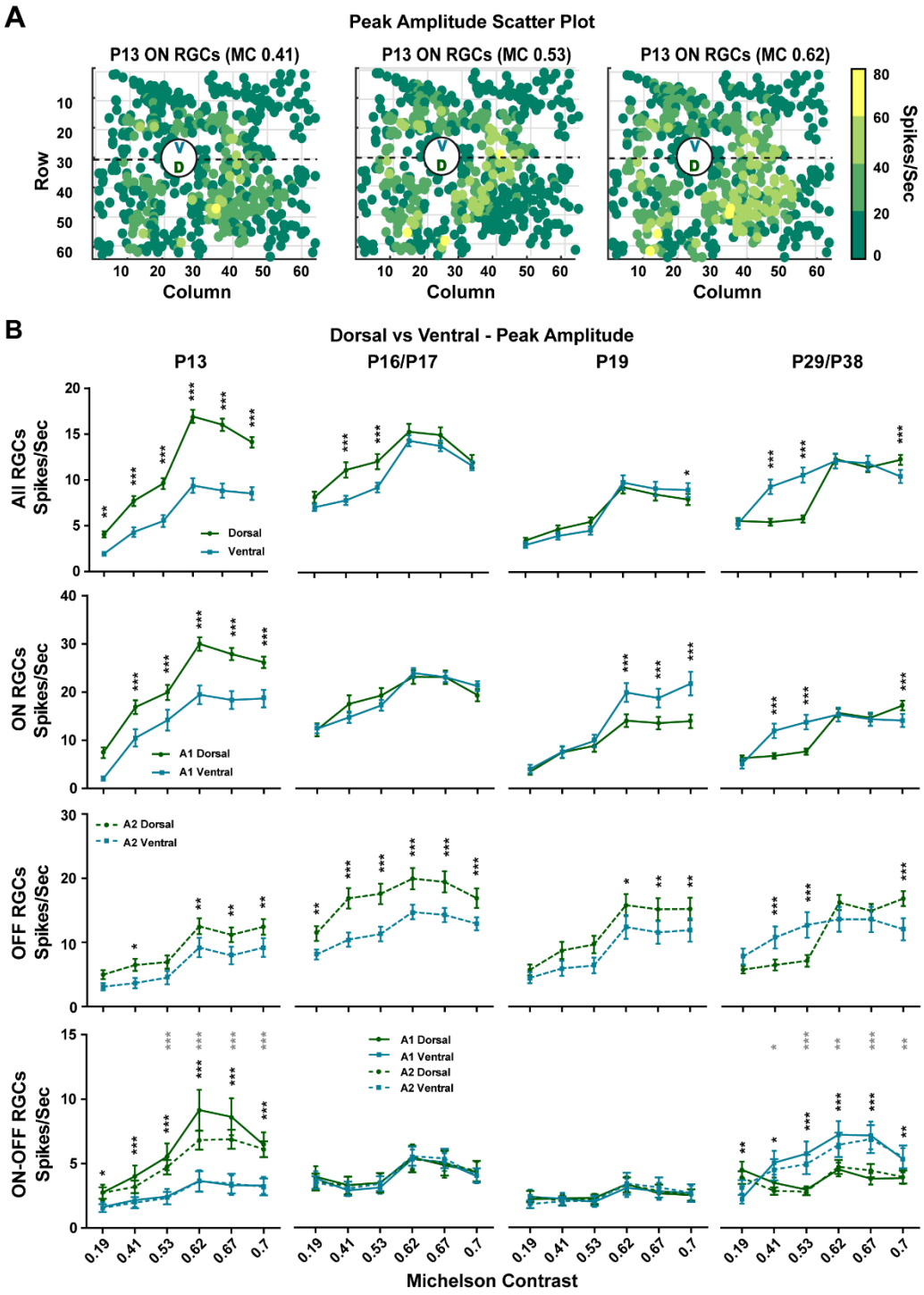

Figure 5

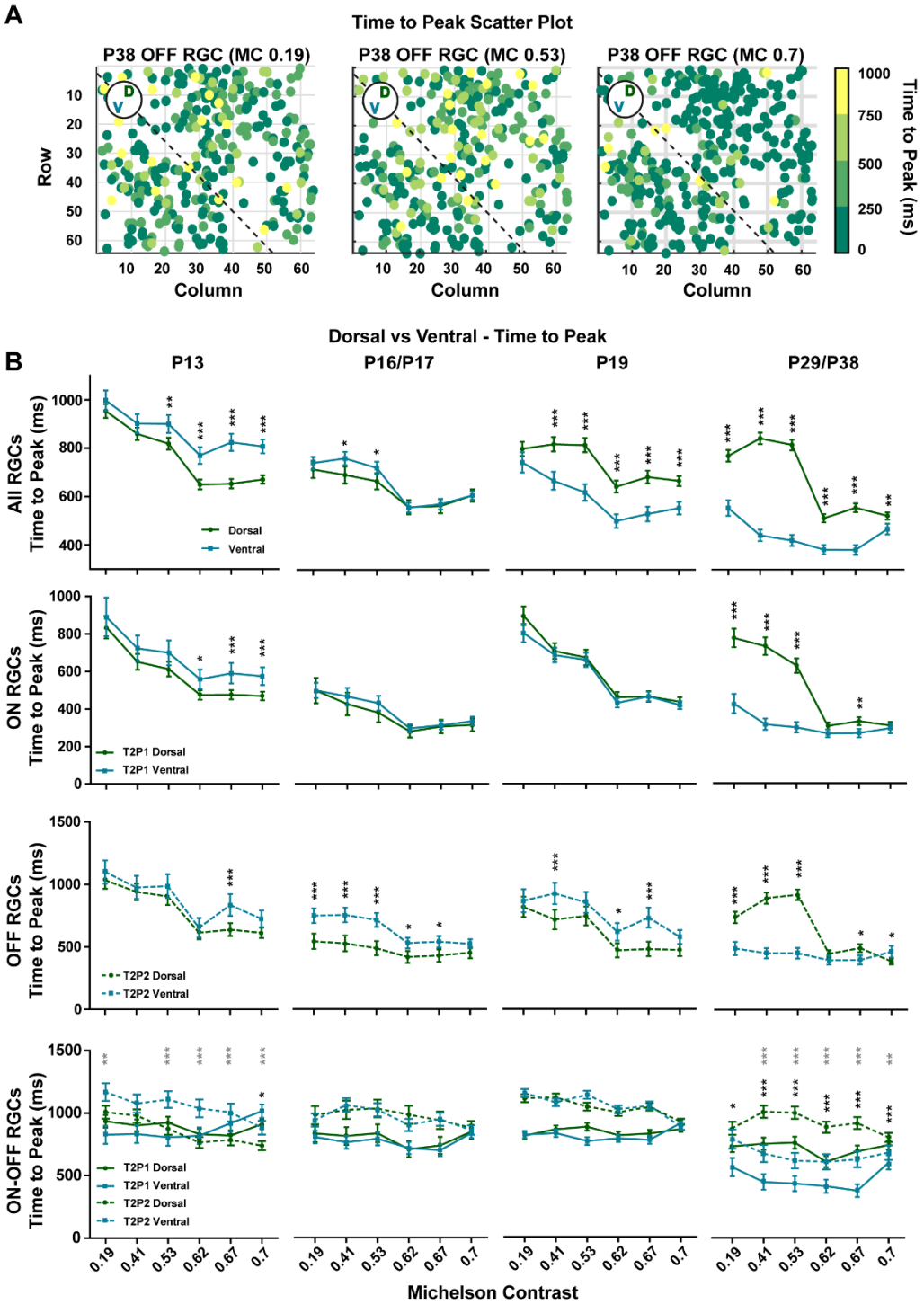

871

872 **Figure 6**

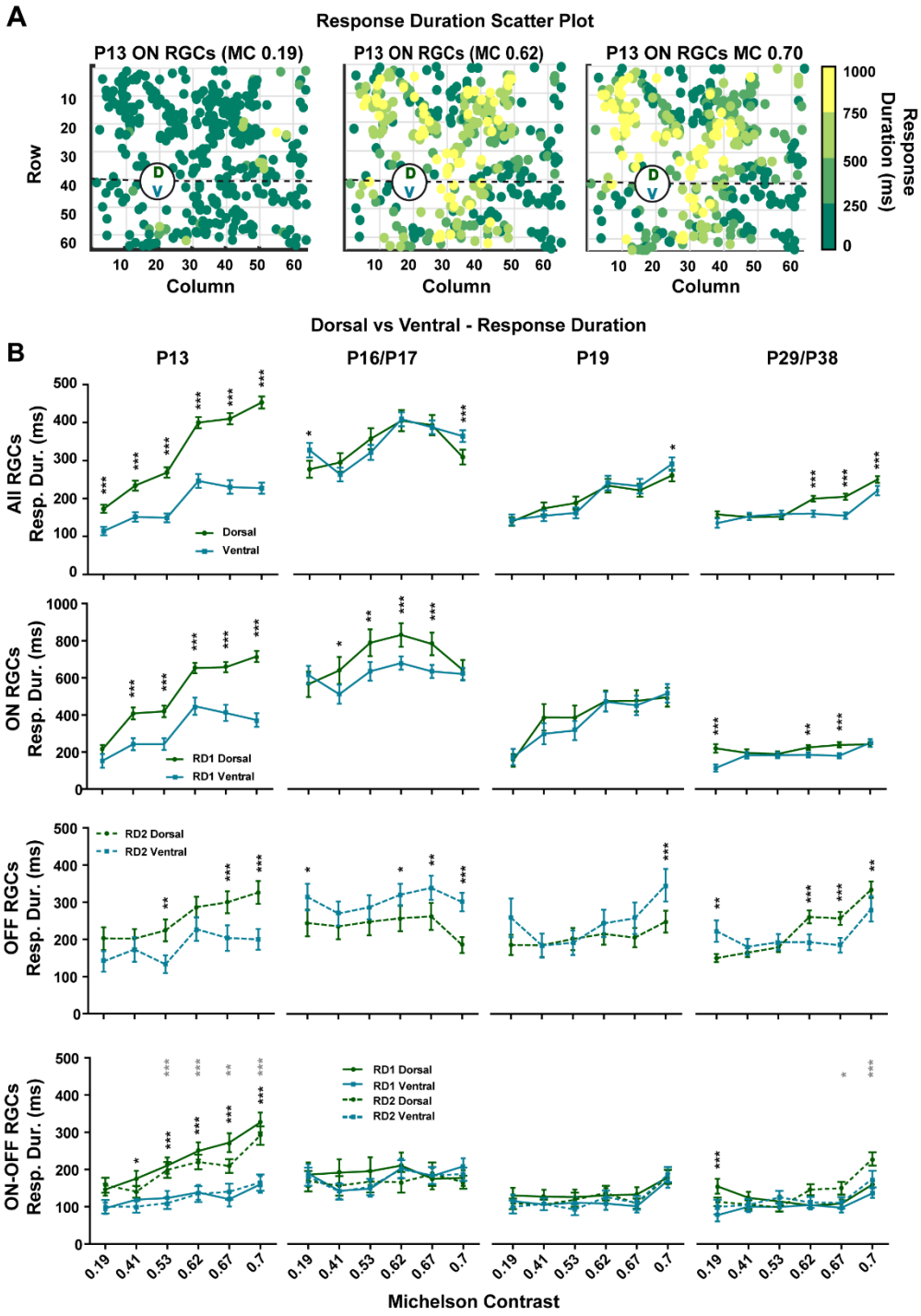

873

874

875

876

877

878

879 **Figure 7**

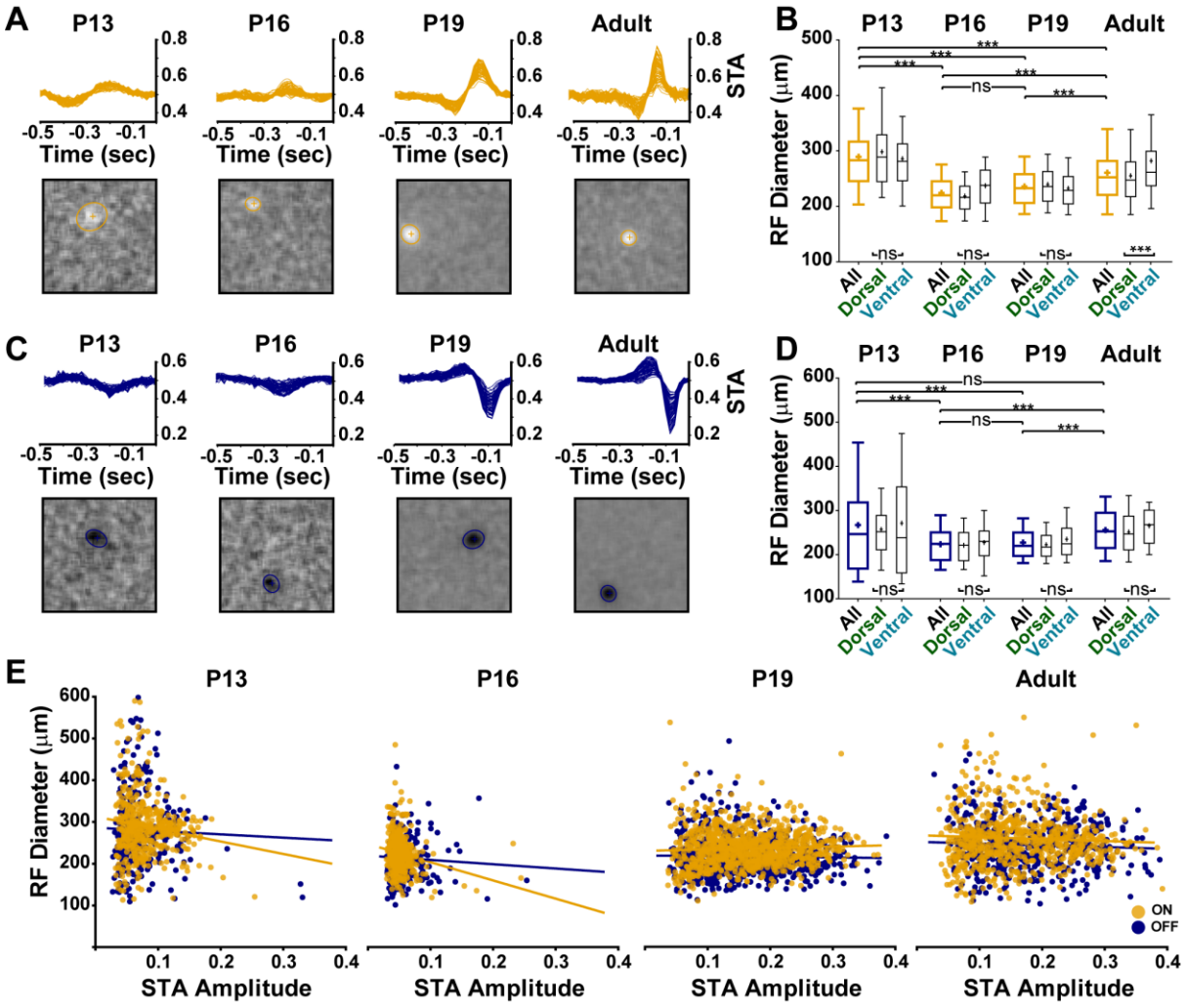

880

881

882

883

884

885 **Mathematics and Equations**

886 $$F = \frac{\sigma_W^2}{\mu_W}$$

887 $$\Pi_P\big(x - X_b - \varepsilon_S(x,t)\big)\Pi_P\big(y - Y_b - \varepsilon_S(y,t)\big)\omega(b,t)$$

$$I_\varepsilon(x,y,t) = \sum_{b=1}^{B}$$